Small signal model of Triangular Current Mode (TCM) operation for Bidirectional Source/Sink Buck and Boost Power Converters

Aitor Vázquez, Kevin Martín, Manuel Arias, Diego G. Lamar, María R. Rogina and Javier Sebastián.
Electronic Power Supply Systems group.
University of Oviedo.
Campus de Viesques s/n, Edificio 3, 33204, Gijon, SPAIN.
vazquezaitor@uniovi.es

***Abstract*— This paper presents a small signal model for bidirectional source/sink buck and boost power converters operating in Triangular Current Mode (TCM) and controlled with a variable-width Hysteretic Current Mode Control (HCMC). The well-known current injected equivalent circuit approach (CIECA) has been applied to derive the canonical circuit. For the sake of simplicity, the resonant intervals during the dead-times have been obtained using a linear approximation. The theoretical small signal model has been validated using two different source/sink power converters: an 80 W synchronous buck converter from 48 V to 24 V and a 100 W synchronous boost converter from 24 V to 48 V. The transfer functions of this power converter have been measured using a Venable Frequency Response Analyzer (FRA6340) and compared to the theoretical ones.**

Keywords*— *Small-signal modelling, Quasi-Square-Wave, Zero-Voltage-Switching, Triangular Current Mode, Hysteretic Current Mode Control, analog control.

I. INTRODUCTION

Many applications require compact, simple, inexpensive and efficient power converters. A very popular operation mode for obtaining these desirable features is the Quasi-Square-Wave Zero-Voltage-Switching (QSW-ZVS) mode [1], also known as Triangular Current Mode (TCM) [2]. ZVS can be achieved thanks to the resonant sub-intervals during the dead-time after the transistor conduction periods [1]–[3].

With properly controlled synchronous rectification instead of a diode, it is possible to maintain ZVS operation even with bidirectional power flow. The ZVS operation can be guaranteed for any power by varying the switching frequency according to the load [4], increasing the switching frequency for lower loads [1], [2]. This soft-switching operation allows either to increase the converter efficiency (for a given size), or to reduce its size (for a given efficiency) by increasing the overall switching frequency for the same power loss. These two properties make this mode very attractive when aiming to obtain a compact and efficient converter.

Source/sink power converters are defined as those bidirectional power converters that regulate the voltage at a given port, independently of the power flow direction, as seen in Fig. 1, where a voltage feedback loop guarantees that the voltage at the output port is constant, at least in steady-state. Some examples of use of bidirectional source/sink power converters

This work was supported by the Science, Innovation and University Ministry of the Spanish Government under Project RTI2018-099682-A-I00, by the Principality of Asturias under the project IDI/2018/000179 and by the European Regional Development Fund (ERDF) grants.

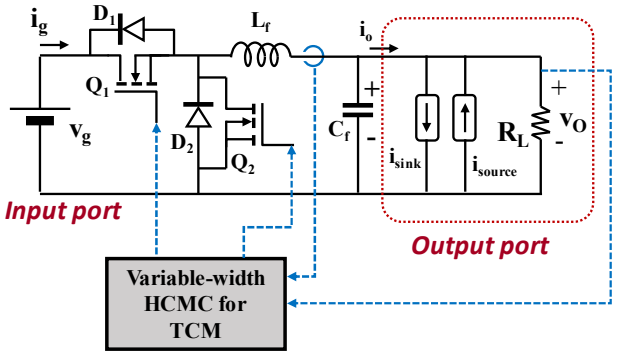

Fig. 1. Output voltage regulated source/sink buck converter supplying active and passive loads.

are the power supplies for Dynamic Digital RAM memories (DDR) [5], [6] or the front-end power converters in dc nano-grids [7]. These converters require high efficiency across widely variable loads, making TCM a very interesting solution. In this paper, the mode of operation is defined from the point of view of the input port. Thus, ***source mode*** corresponds to power going from the input port to the output port, with the load behaving as a sink. ***Sink mode*** corresponds to power going from the output port to the input port, with the load behaving as a source.

Even though the TCM has been analyzed in detail in [1-4], neither of these works has dealt with the dynamic model of the source/sink behavior, nor with a variable-width Hysteretic Current Mode Controller (HCMC). Due to the different types of loads that can be connected to the output port, it is mandatory to know the dynamics of the converter in both source/sink modes. In order to overcome this lack, this paper presents two small signal models for the converter shown in Fig. 1 when operating in either source or sink modes with a variable-width HCMC: a complete model valid across all loading conditions and a simpler one only valid at heavy loads.

II. REVIEW OF THE STEADY STATE ANALISYS OF THE BUCK CONVERTER OPERATING IN SOURCE MODE AND WITH VARIABLE-WIDTH HCMC FOR TCM OPERATION

Fig. 2 shows the equivalent circuit corresponding to the converter given in Fig. 1. The operation of transistors Q_1 and Q_2 has been approximated as ideal switches S_1 and S_2 with parasitic capacitances C_{p1} and C_{p2}. In order to achieve ZVS, the value of

i_{Lf} (the current through filter inductor L_f) is controlled as shown in Fig. 3. Thus, transistor Q_1 is turned off when i_{Lf} reaches a specific value i_p determined by the control circuit. After a time delay labelled as t_{dR1} in Fig. 3, transistor Q_2 is turned on. It should be noted that t_{dR1} must be wide enough to guarantee the discharge of capacitor C_{p2} (from v_g to 0) and the charge of capacitor C_{p1} (from v_g to 0). This is a resonant process, which takes place during interval (t_2, t_3). In order to guarantee ZVS operation, (t_2-t_1) < t_{dR1} in any operating condition.

Similarly, a resonant transition occurs at the end of the conduction period corresponding to Q_2. In this case (source mode operation), the turn off of Q_2 occurs when i_{Lf} reaches -I_v, which is determined in order to make possible ZVS operation for any possible combination of v_g and v_o values. Although both i_p and I_v determine the turn-off of a transistor (Q_1 in the case of i_p and Q_2 in the case of I_v), it should be noted that there is a big difference between them: i_p is a variable (in fact is the control variable in source mode), whereas I_v is a constant value determined in the design process [8]. Once transistor Q_2 is turned off, another resonant period starts. It takes place during interval (t_4, t_5). As in the previous resonant period, a time delay between the turn-off of Q_2 and the turn-on of Q_1 must be programmed in order to guarantee ZVS operation. This is the time period labelled as t_{dR2} in Fig. 3. As in the previous case, it must be guaranteed that (t_5-t_4) < t_{dR2} for any possible situation.

The detailed analysis of the converter operation gives six operation intervals:

- ***Interval (t_0, t_1):*** after turning on the transistor Q_1 before t_0, i_{Lf} becomes positive at t_0. From t_0 to t_1, current i_{Lf} is conducted by

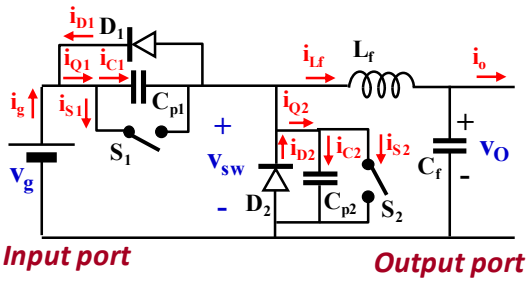

Fig. 2. Equivalent circuit for the converter shown in Fig. 1.

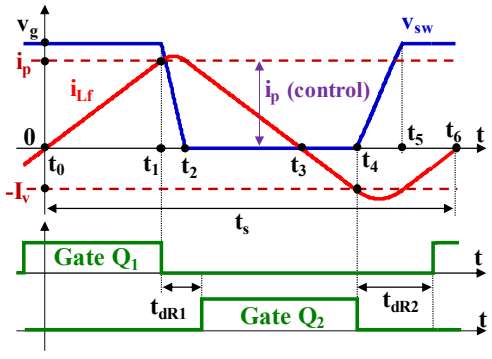

Fig. 3. Main waveforms corresponding to the equivalent circuit given in Fig. 2 working in source mode.

Q_1 (actually by S_1 in the equivalent model of Fig. 3). According to Faraday's law:

$$i_{Lf} = \frac{v_g - v_o}{L_f}(t - t_0). \quad (1)$$

The end of this interval is reached at:

$$t_1 = t_0 + \frac{L_f \cdot i_p}{v_g - v_o}, \quad (2)$$

which is determined by the control signal i_p. The voltage across the switching node is:

$$v_{sw} = v_g. \quad (3)$$

- ***Interval (t_1, t_2):*** the gate signal of Q_1 is turned off just at t_1 and Q_2 is not turned on yet. This means that both ideal switches S_1 and S_2 are open in the equivalent circuit of Fig. 2. As a consequence, a resonant period starts at this moment. To study this period, we are going to define the following parameters:

$$C_T = C_{p1} + C_{p2}, \quad (4)$$

$$\omega_R = \frac{1}{\sqrt{L_f \cdot C_T}}, \quad (5)$$

$$Z_C = \sqrt{\frac{L_f}{C_T}}, \quad (6)$$

where C_T is the parallel equivalent output capacitance of both transistors, ω_R is the resonant angular frequency and Z_C is the characteristic impedance. The analysis of this circuit leads to the following equations:

$$i_{Lf} = \frac{v_g - v_o}{Z_C}\sin[\omega_R(t - t_1)] + i_p \cos[\omega_R(t - t_1)], \quad (7)$$

$$v_{sw} = v_o + (v_g - v_o)\cos[\omega_R(t - t_1)] + i_p Z_C \sin[\omega_R(t - t_1)]. \quad (8)$$

The end of this interval is reached when $v_{sw} = 0$. From (8) we obtain:

$$t_2 = t_1 + \frac{arcsin\left[\frac{-b_1 + \sqrt{b_1^2 - 4a_1 c_1}}{2a_1}\right]}{\omega_R}, \quad (9)$$

where:

$$a_1 = (i_p Z_C)^2 + (v_g - v_o)^2, \quad (10)$$

$$b_1 = -2 i_p Z_C v_o, \quad (11)$$

$$c_1 = 2 v_g (v_o - v_g). \quad (12)$$

The value of i_{Lf} at the end of this interval can be easily obtained by replacing t with t_2 in (7). This value will be labelled as $i_{Lf\text{-}t2}$.

The electric charge interchanged between C_{p1} and C_{p2} during this resonant period can be calculated as follows:

$$q_{R1} = \int_{t_1}^{t_2} i_{Lf} dt. \quad (13)$$

This calculation yields:

$$q_{R1} = C_T v_g. \quad (14)$$

This is an interesting and logical conclusion: the electric charge interchanged between both capacitors only depends on

their equivalent capacitance and on the voltage variation across them.

- ***Interval (t_2, t_3):*** when v_{sw} reaches 0 at t_2, i_{Lf} is conducted by diode D_2, thus starting a new period of operation. Q_2 will be turned on in any time instant between t_2 and t_3. However, a delay time must be stablished in order to achieve ZVS even in the worst conditions. This delay time t_{dR1} can be computed as:

$$t_{dR1} = t_{2max} - t_1, \tag{15}$$

where the value of t_{2max} can be computed from (9)-(12) when the converter is operating at maximum input voltage v_{gmax}, maximum output voltage v_{omax}, and minimum (critical) value of control variable i_p, i_{pcrit}.

The values of i_{Lf} and v_{sw} in this interval can be computed as in interval (t_0, t_1). The results are:

$$i_{Lf} = i_{Lf-t2} - \frac{v_o}{L_f}(t - t_2), \tag{16}$$

$$v_{sw} = 0. \tag{17}$$

The end of this interval occurs when $i_{Lf} = 0$, just at t_3. Its value can be easily computed from (16) as follows:

$$t_3 = t_2 + \frac{L_f \cdot i_{Lf-t2}}{v_o}. \tag{18}$$

- ***Interval (t_3, t_4):*** this interval starts when $i_{Lf} < 0$, which means that current i_{Lf} cannot be conducted by D_2 and must be conducted by Q_2 (S_2 in the circuit of Fig. 2). The interval ends when i_{Lf} reaches a programed negative value $-I_v$. This value must be adequate to guarantee ZVS operation during the next interval (the resonant interval (t_4, t_5)). Equations (16) and (17) describe the operation in this mode. The end of this interval takes place at:

$$t_4 = t_3 + \frac{L_f \cdot I_v}{v_o}. \tag{19}$$

- ***Interval (t_4, t_5):*** this is the second resonant interval. As mentioned above, it starts when $i_{Lf} = -I_v$ and ends when capacitors C_{p1} and C_{p2} interchange their electric charge. The analysis of this interval is very similar to the one corresponding to interval (t_1, t_2). The final results are the following:

$$i_{Lf} = \frac{-v_o}{Z_C}\sin[\omega_R(t - t_4)] - I_v \cos[\omega_R(t - t_4)], \tag{20}$$

$$v_{sw} = v_o - v_o \cos[\omega_R(t - t_4)] + I_v Z_C \sin[\omega_R(t - t_4)]. \tag{21}$$

The end of this interval is reached when $v_{sw} = v_g$. Replacing v_{sw} with v_g in (21), we obtain:

$$t_5 = t_4 + \frac{arccos\left[\frac{-b_2 + \sqrt{{b_2}^2 - 4a_2 c_2}}{2a_2}\right]}{\omega_R}, \tag{22}$$

where:

$$a_2 = (I_v Z_C)^2 + {v_o}^2, \tag{23}$$

$$b_2 = 2v_o(v_g - v_o), \tag{24}$$

$$c_2 = -(I_v Z_C)^2 + (v_g - v_o)^2. \tag{25}$$

It should be noted that ZVS operation is obtained only if v_{sw} reaches v_g at the end of this interval, which implies a real solution for (21). This is only possible if:

$${b_2}^2 - 4a_2 c_2 \geq 0. \tag{26}$$

From (26), and considering (23)-(25), ZVS is achieved if:

$$I_v \geq \sqrt{\frac{v_g(v_g - 2v_o)}{{Z_C}^2}}. \tag{27}$$

It should be noted that (27) only makes sense if $v_g > 2v_o$. This is because ZVS can be obtained without a negative value of i_{Lf} if $v_g < 2v_o$. In summary, taking into account the variation of v_g and v_o, ZVS is achieved if:

$$I_v \geq I_{vcrit}, \tag{28}$$

I_{vcrit} being:

- $I_{vcrit} = 0$ if $v_{gmax} \leq 2v_{omin}$, (29)
- $I_{vcrit} = \sqrt{\frac{v_{gmax}(v_{gmax} - 2v_{omin})}{{Z_C}^2}}$ if $v_{gmax} > 2v_{omin}$. (30)

In this paper, only the case corresponding to (30) is considered, as it is the more general case.

The value of i_{Lf} at the end of this interval can be easily obtained by replacing t with t_5 in (20). This value will be labelled as $i_{Lf\text{-}t5}$.

The electric charge interchanged between C_{p1} and C_{p2} during this resonant period can be calculated as follows:

$$q_{R2} = \int_{t_4}^{t_5} i_{Lf}\, dt. \tag{31}$$

This calculation yields:

$$q_{R2} = -C_T v_g = -q_{R1}, \tag{32}$$

which means that the same amount of electric charge is interchanged between the capacitors in both resonant periods.

- ***Interval (t_5, t_6):*** when v_{sw} reaches v_g at t_5, i_{Lf} is conducted by diode D_1. Transistor Q_1 will be turned on again at any time instant between t_5 and t_6, t_6 being the end of the switching period. However, a delay time between Q_2 turn-off and Q_1 turn-on must be stablished in order to achieve ZVS in any condition. This delay time t_{dR2} can be computed as:

$$t_{dR2} = t_{5max} - t_4, \tag{33}$$

where the value of t_{5max} can be calculated from (22)-(25), by replacing v_g with v_{gmax}, v_o with v_{omin} and I_v with I_{vcrit}.

The values of i_{Lf} and v_{sw} in this interval can be computed as in interval (t_0, t_1). The results are:

$$i_{Lf} = i_{Lf-t5} + \frac{v_g - v_o}{L_f}(t - t_5), \tag{34}$$

$$v_{sw} = v_g. \tag{35}$$

The end of this interval will be at:

$$t_6 = t_5 - \frac{L_f \cdot i_{Lf-t5}}{v_g - v_o}. \tag{36}$$

Finally, the switching period is:

$$t_s = t_6 - t_0. \tag{37}$$

To obtain an average small signal model, the evaluation of the average current injected into the output port and the average current drained from the input port have to be analyzed. These average currents can in turn be computed from the electric charge injected into and drained from those ports (q_{inj} and q_g):

$$q_{inj} = q_{01} + q_{R1} + q_{23} + q_{34} + q_{R2} + q_{56}. \quad (38)$$

$$q_g = q_{01} + \frac{q_{R1}}{2} + \frac{q_{R2}}{2} + q_{56}\ , \quad (39)$$

where:

$$q_{01} = \int_{t_0}^{t_1} i_{Lf} dt, \quad (40)$$

$$q_{23} = \int_{t_2}^{t_3} i_{Lf} dt, \quad (41)$$

$$q_{34} = \int_{t_3}^{t_4} i_{Lf} dt, \quad (42)$$

$$q_{56} = \int_{t_5}^{t_6} i_{Lf} dt. \quad (43)$$

After taking into account (32), equations (38) and (39) become:

$$q_{inj} = q_{01} + q_{23} + q_{34} + q_{56}, \quad (44)$$

$$q_g = q_{01} + q_{56}. \quad (45)$$

Once the electric charges are known, the average current injected into the output capacitor C_f and the load, i_{inj}, and drained from the input voltage source placed at the input port, i_g, can be easily calculated:

$$i_{inj} = \frac{q_{inj}}{t_s}, \quad (46)$$

$$i_g = \frac{q_g}{t_s}. \quad (47)$$

Equations (46) and (47) are the starting points to develop an average, small-signal model for this converter.

III. Dynamic Analisys of the Buck Converter Operating in Source Mode and with Variable-Width HCMC for TCM Operation

A. Complete model.

A simple, average small-signal model can be obtained by perturbing (46) and (47) around a steady-state point. As the control method programs the current passing through the inductor and this current is reset each switching cycle, a first order model is expected. Due to this, the Current Injected Equivalent Circuit Approach (CIECA) [9] model is used in this paper. The steady-state values of the different quantities will be written in capital letters, while the perturbed values will be written in lower-case with "hats". The relationship between the actual, the steady-state and the perturbed values are as follows:

$$v_g = V_g + \hat{v}_g, \quad (48)$$

$$v_o = V_o + \hat{v}_o, \quad (49)$$

$$i_p = I_p + \hat{\imath}_p, \quad (50)$$

$$t_s = T_s + \hat{t}_s, \quad (51)$$

$$q_{inj} = Q_{inj} + \hat{q}_{inj}, \quad (52)$$

$$q_g = Q_g + \hat{q}_g. \quad (53)$$

Perturbing (46) and (47), we obtain:

$$\hat{\imath}_{inj} = G_{ivg}\hat{v}_g + G_{ivo}\hat{v}_o + G_{iip}\hat{\imath}_p, \quad (54)$$

$$\hat{\imath}_g = G_{gvg}\hat{v}_g + G_{gvo}\hat{v}_o + G_{gip}\hat{\imath}_p, \quad (55)$$

where:

$$G_{ivg} = \frac{\partial i_{inj}}{\partial v_g}\Big]_0 = \frac{\partial\left[\frac{q_{inj}}{t_s}\right]}{\partial v_g}\Big]_0, \quad (56)$$

$$G_{ivo} = -\frac{1}{r_2} = \frac{\partial i_{inj}}{\partial v_o}\Big]_0 = \frac{\partial\left[\frac{q_{inj}}{t_s}\right]}{\partial v_o}\Big]_0, \quad (57)$$

$$G_{iip} = \frac{\partial i_{inj}}{\partial i_p}\Big]_0 = \frac{\partial\left[\frac{q_{inj}}{t_s}\right]}{\partial i_p}\Big]_0, \quad (58)$$

$$G_{gvg} = \frac{1}{r_1} = \frac{\partial i_g}{\partial v_g}\Big]_0 = \frac{\partial\left[\frac{q_g}{t_s}\right]}{\partial v_g}\Big]_0, \quad (59)$$

$$G_{gvo} = \frac{\partial i_g}{\partial v_o}\Big]_0 = \frac{\partial\left[\frac{q_g}{t_s}\right]}{\partial v_o}\Big]_0, \quad (60)$$

$$G_{gip} = \frac{\partial i_g}{\partial i_p}\Big]_0 = \frac{\partial\left[\frac{q_g}{t_s}\right]}{\partial i_p}\Big]_0. \quad (61)$$

As a result of using this approach, the first-order small-signal linear equivalent circuit given in Fig. 4 can be obtained from (54) and (55). However, the values of these G parameters cannot be easily obtained, due to complexity of the equation needed to calculate time intervals, especially those related to t_2 and t_5. It should be noted that t_2 depends on v_g, v_o and i_p (see (9-12)) and t_5 depends on v_g, and v_o (see (22-25)). Moreover, other time intervals also depend on these variables. As a consequence, the switching frequency t_s and the electric charges previously calculated also depend on those variables, making it impossible to obtain analytical expressions for the above-mentioned G parameters. Therefore, a simplified model must be developed.

B. Simplified model for light and heavy load

Fig. 5 shows the simplified version of the inductor current i_{Lf} that is going to be considered in this subsection. As this figure shows, i_{Lf} is supposed to be constant during the resonant intervals (t_2, t_1) and (t_4, t_5). The values of i_{Lf} in these intervals are i_p and $-I_{vcrit}$, respectively. The length of these intervals is adjusted in such a way that the values of the electric charges q_{R1} and q_{R2} are equal to the those given in (14) and (32). Therefore, (9) and (22) can be re-written now as follows:

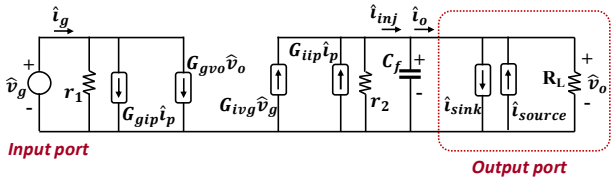

Fig. 4. Canonical model for the converter.

$$t_2 = t_1 + \frac{v_g}{i_p} C_T, \tag{62}$$

$$t_5 = t_4 + v_g \frac{C_T}{I_{vcrit}}. \tag{63}$$

These simplifications make the task of calculating the above-mentioned G parameters affordable. Thus, the electric charges shown in Fig.4 can easily computed as follows:

$$q_{01} = \frac{L_f}{2} \cdot \frac{{i_p}^2}{v_g - v_o}, \tag{64}$$

$$q_{23} = \frac{L_f}{2} \cdot \frac{{i_p}^2}{v_o}, \tag{65}$$

$$q_{34} = -\frac{L_f {I_{vcrit}}^2}{2} \cdot \frac{1}{v_o}, \tag{66}$$

$$q_{56} = -\frac{L_f {I_{vcrit}}^2}{2} \cdot \frac{1}{v_g - v_o}, \tag{67}$$

and then (44) and (45) become:

$$q_{inj} = \frac{L_f}{2}({i_p}^2 - {I_{vcrit}}^2)\left[\frac{1}{v_g - v_o} + \frac{1}{v_o}\right], \tag{68}$$

$$q_g = \frac{L_f}{2}({i_p}^2 - {I_{vcrit}}^2)\left[\frac{1}{v_g - v_o}\right]. \tag{69}$$

Regarding the equations concerning time, (2) remains valid now, but equations for t_3, t_4 and t_6 changes as follows:

$$t_3 = t_2 + \frac{L_f \cdot i_p}{v_o}, \tag{70}$$

$$t_4 = t_3 + \frac{L_f \cdot I_{vcrit}}{v_o}, \tag{71}$$

$$t_6 = t_5 + \frac{L_f \cdot I_{vcrit}}{v_g - v_o}. \tag{72}$$

Finally, the switching period can be easily obtained from (37), considering (2), (62), (63), (70), (71) and (72). The result is:

$$t_s = L_f\left(I_{vcrit} + i_p\right)\left[\frac{1}{v_g - v_o} + \frac{1}{v_o}\right] + v_g C_T \left[\frac{1}{I_{vcrit}} + \frac{1}{i_p}\right]. \tag{73}$$

Now, the value of the G parameters of the canonical model can be computed as follows:

$$G_{ivg} = \left.\frac{\partial\left[\frac{q_{inj}}{t_s}\right]}{\partial v_g}\right]_0 = \left.\frac{1}{T_s}\frac{\partial q_{inj}}{\partial v_g}\right]_0 - \left.\frac{Q_{inj}}{{T_s}^2}\frac{\partial t_s}{\partial v_g}\right]_0, \tag{74}$$

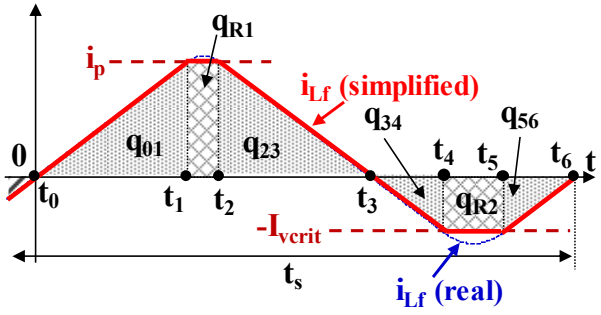

Fig. 5. Simplified approach of the inductor current waveform used to obtain the simplified small-signal average model.

$$G_{ivo} = -\frac{1}{r_2} = \left.\frac{\partial\left[\frac{q_{inj}}{t_s}\right]}{\partial v_o}\right]_0 = \left.\frac{1}{T_s}\frac{\partial q_{inj}}{\partial v_o}\right]_0 - \left.\frac{Q_{inj}}{{T_s}^2}\frac{\partial t_s}{\partial v_o}\right]_0, \tag{75}$$

$$G_{iip} = \left.\frac{\partial\left[\frac{q_{inj}}{t_s}\right]}{\partial i_p}\right]_0 = \left.\frac{1}{T_s}\frac{\partial q_{inj}}{\partial i_p}\right]_0 - \left.\frac{Q_{inj}}{{T_s}^2}\frac{\partial t_s}{\partial i_p}\right]_0, \tag{76}$$

$$G_{gvg} = \frac{1}{r_1} = \left.\frac{\partial\left[\frac{q_g}{t_s}\right]}{\partial v_g}\right]_0 \left.\frac{1}{T_s}\frac{\partial q_g}{\partial v_g}\right]_0 - \left.\frac{Q_g}{{T_s}^2}\frac{\partial t_s}{\partial v_g}\right]_0, \tag{77}$$

$$G_{gvo} = \left.\frac{\partial\left[\frac{q_g}{t_s}\right]}{\partial v_o}\right]_0 = \left.\frac{1}{T_s}\frac{\partial q_g}{\partial v_o}\right]_0 - \left.\frac{Q_g}{{T_s}^2}\frac{\partial t_s}{\partial v_o}\right]_0, \tag{78}$$

$$G_{gip} = \left.\frac{\partial\left[\frac{q_g}{t_s}\right]}{\partial i_p}\right]_0 = \left.\frac{1}{T_s}\frac{\partial q_g}{\partial i_p}\right]_0 - \left.\frac{Q_g}{{T_s}^2}\frac{\partial t_s}{\partial i_p}\right]_0. \tag{79}$$

where:

$$T_s = L_f\left(I_{vcrit} + I_p\right)\left[\frac{1}{V_g - V_o} + \frac{1}{V_o}\right] + V_g C_T \left[\frac{1}{I_{vcrit}} + \frac{1}{I_p}\right], \tag{80}$$

$$Q_{inj} = \frac{L_f}{2}({I_p}^2 - {I_{vcrit}}^2)\left[\frac{1}{V_g - V_o} + \frac{1}{V_o}\right], \tag{81}$$

$$Q_g = \frac{L_f}{2}({I_p}^2 - {I_{vcrit}}^2)\left[\frac{1}{V_g - V_o}\right], \tag{82}$$

$$\left.\frac{\partial q_{inj}}{\partial v_g}\right]_0 = -\frac{L_f}{2} \cdot \frac{{I_p}^2 - {I_{vcrit}}^2}{(V_g - V_o)^2}, \tag{83}$$

$$\left.\frac{\partial q_{inj}}{\partial v_o}\right]_0 = \frac{L_f}{2} \cdot ({I_p}^2 - {I_{vcrit}}^2)\left[\frac{1}{(V_g - V_o)^2} + \frac{1}{{V_o}^2}\right], \tag{84}$$

$$\left.\frac{\partial q_{inj}}{\partial i_p}\right]_0 = \frac{L_f I_p V_g}{(V_g - V_o)V_o}, \tag{85}$$

$$\left.\frac{\partial q_g}{\partial v_g}\right]_0 = -\frac{L_f}{2} \cdot \frac{{I_p}^2 - {I_{vcrit}}^2}{(V_g - V_o)^2} = \left.\frac{\partial q_{inj}}{\partial v_g}\right]_0, \tag{86}$$

$$\left.\frac{\partial q_g}{\partial v_o}\right]_0 = \frac{L_f}{2} \cdot \frac{{I_p}^2 - {I_{vcrit}}^2}{(V_g - V_o)^2} = -\left.\frac{\partial q_{inj}}{\partial v_g}\right]_0, \tag{87}$$

$$\left.\frac{\partial q_g}{\partial i_p}\right]_0 = \frac{L_f I_p}{(V_g - V_o)}, \tag{88}$$

$$\left.\frac{\partial t_s}{\partial v_g}\right]_0 = -L_f \frac{I_p - I_{vcrit}}{(V_g - V_o)^2} + C_T \left[\frac{1}{I_{vcrit}} + \frac{1}{I_p}\right], \tag{89}$$

$$\left.\frac{\partial t_s}{\partial v_o}\right]_0 = L_f(I_p - I_{vcrit})\left[\frac{1}{(V_g - V_o)^2} - \frac{1}{{V_o}^2}\right], \tag{90}$$

$$\left.\frac{\partial t_s}{\partial i_p}\right]_0 = L_f\left[\frac{1}{V_g - V_o} + \frac{1}{V_o}\right] - \frac{C_T V_g}{{I_p}^2}. \tag{91}$$

Substituting (80)-(91) into (74) - (79), we finally obtain:

$$G_{ivg} = -\frac{1}{{\omega_R}^2} \cdot \frac{F_0 V_o}{I_p I_{vcrit}}, \tag{92}$$

$$G_{ivo} = -\frac{1}{r_2} = \frac{1}{{\omega_R}^2} \cdot \frac{F_0(2V_o - V_g)}{I_p I_{vcrit}}, \tag{93}$$

$$G_{iip} = {L_f}^2 \frac{F_0}{I_p - I_{vcrit}}\left[1 + \frac{(V_g - V_o)V_o(2I_p - I_{vcrit})}{{Z_c}^2 {I_p}^2 I_{vcrit}}\right], \tag{94}$$

$$G_{gvg} = \frac{1}{r_1} = -{L_f}^2 \frac{F_0 V_o}{{V_g}^2}\left[1 + \frac{(2V_g - V_o)V_o}{{Z_c}^2 I_p I_{vcrit}}\right], \tag{95}$$

$$G_{gvo} = {L_f}^2 \frac{F_0}{V_g}\left[1 + \frac{{V_o}^2}{{Z_c}^2 {I_p} I_{vcrit}}\right], \quad (96)$$

$$G_{gip} = {L_f}^2 \frac{F_0 V_o}{V_g (I_p - I_{vcrit})}\left[1 + \frac{(V_g - V_o)V_o(2I_p - I_{vcrit})}{{Z_c}^2 {I_p}^2 I_{vcrit}}\right], \quad (97)$$

where:

$$F_0 = \frac{1}{2{T_s}^2} \cdot \frac{(I_p + I_{vcrit})^2 (I_p - I_{vcrit}) {V_g}^2}{(V_g - V_o)^2 {V_o}^2}. \quad (98)$$

Equation (93) shows that the value of r_2 can be either positive ($2V_o < V_g$) or negative ($2V_o > V_g$). Regarding r_1, (95) shows that it is always negative, as expected (when i_p is constant, the power handled by the converter is almost constant and, therefore, the input current decreases when the input voltage increases).

C. Simplified model for heavy load

Figure 6 shows the typical inductor current waveforms corresponding to operation at full load. In this case, the converter operates at the lowest switching frequency and the resonant intervals are negligible, i.e., $\omega_R >> 2\pi/T_s$ and $2\pi L_f/T_s >> Z_c$. These relationships means that $\lambda \rightarrow 0$ if λ is defined as $\lambda = 2\pi/(T_s \omega_R)$. Moreover, I_{vcrit} is also negligible in comparison to i_p. Due to this, a pure triangular waveform can be considered. Equation (80) becomes now:

$$T_s = \frac{L_f I_p V_g}{(V_g - V_o)V_o}. \quad (99)$$

Taking into account (5), (6), (30) and (99), the following limits can be easily calculated from the values given in (92)-(98):

$$G_{ivg\_hl} = \lim_{\lambda \to 0} G_{ivg} = 0, \quad (100)$$

$$G_{ivo\_hl} = -\frac{1}{r_2} = \lim_{\lambda \to 0} G_{ivo} = 0, \quad (101)$$

$$G_{iip\_hl} = \lim_{\lambda \to 0} G_{iip} = \frac{1}{2}, \quad (102)$$

$$G_{gvg\_hl} = \frac{1}{r_1} = \lim_{\lambda \to 0} G_{gvg} = -\frac{1}{R_o}\left(\frac{V_o}{V_g}\right)^2, \quad (103)$$

$$G_{gvo\_hl} = \lim_{\lambda \to 0} G_{gvo} = \frac{1}{R_o}\left(\frac{V_o}{V_g}\right), \quad (104)$$

$$G_{gip\_hl} = \lim_{\lambda \to 0} G_{gip} = \frac{1}{2}\left(\frac{V_o}{V_g}\right), \quad (105)$$

where:

$$R_0 = \frac{V_o}{I_o}, \quad (106)$$

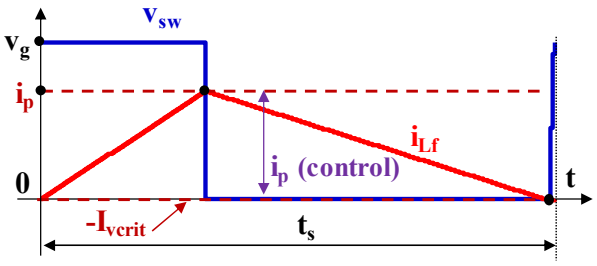

Fig. 6. Main operating waveforms at heavy load in source mode.

$$I_o = \frac{I_p}{2}, \quad (107)$$

I_o being the static value of i_o (see Fig. 2). It should be noted that R_o and R_L are only equal if the load is purely resistive, without any current source or sink in parallel.

D. Transfer functions

Once the values of the G parameters have been obtained, the transfer functions can be directly obtained from Fig. 4 and from these G parameters. Expressions become simpler by defining R_{eq} as follows:

$$R_{eq} = \frac{R_L r_2}{R_L + r_2}. \quad (108)$$

The transfer function between the input and output voltage variations will be:

$$\left.\frac{\hat{v}_o}{\hat{v}_g}\right]_{\substack{\hat{\imath}_p=0 \\ \hat{\imath}_{sink}=0 \\ \hat{\imath}_{source}=0}} = \frac{G_{ivg} R_{eq}}{1 + R_{eq} C_f s}, \quad (109)$$

and the transfer function between the control variable variations and output voltage variations will be:

$$\left.\frac{\hat{v}_o}{\hat{\imath}_p}\right]_{\substack{\hat{v}_g=0 \\ \hat{\imath}_{sink}=0 \\ \hat{\imath}_{source}=0}} = \frac{G_{iip} R_{eq}}{1 + R_{eq} C_f s}. \quad (110)$$

The values of G_{ivg}, r_2 and G_{iip} can be either those corresponding to (92), (93) and (94) for any load or those in (100), (101) and (102) for heavy load only.

IV. Operation in Sink Mode and Extension to the Boost Converter

A similar study as the one made for source mode can be developed for the operation in sink mode. In this case, a current source, as the one drawn in Fig. 1 (labelled as i_{source}), is injecting current into the output port. As Fig. 7 shows, current i_{Lf} is now controlled by variable i_v, which roughly determines the negative peak value of i_{Lf}. In fact, transistor Q_2 turns off when $i_{Lf} = -i_v$, i_v being a positive value. Regarding transistor Q_1, it turns off when $i_{Lf} = I_{pcrit}$. The value of I_{pcrit} is determined by the same equations as I_{vcrit} in source mode (29), (30). In the case of heavy load, the waveforms can be approximated by those shown in Fig. 8.

Regarding the average small-signal modeling, the canonical circuit shown in Fig.4 is also valid in this case, merely replacing $\hat{\imath}_p$ with $\hat{\imath}_v$. Applying the same procedure detailed in Section III, G parameters can now be re-calculated as follows:

$$G_{ivg} = -\frac{1}{{\omega_R}^2} \cdot \frac{F_0 V_o}{I_v I_{pcrit}}, \quad (111)$$

$$G_{ivo} = -\frac{1}{r_2} = \frac{1}{{\omega_R}^2} \cdot \frac{F_0 (2V_o - V_g)}{I_v I_{pcrit}}, \quad (112)$$

$$G_{iiv} = {L_f}^2 \frac{F_0}{I_v - I_{pcrit}}\left[1 + \frac{(V_g - V_o)V_o(2I_v - I_{pcrit})}{{Z_c}^2 {I_v}^2 I_{pcrit}}\right], \quad (113)$$

$$G_{gvg} = \frac{1}{r_1} = -{L_f}^2 \frac{F_0 V_o}{{V_g}^2}\left[1 + \frac{(2V_g - V_o)V_o}{{Z_c}^2 I_v I_{pcrit}}\right], \quad (114)$$

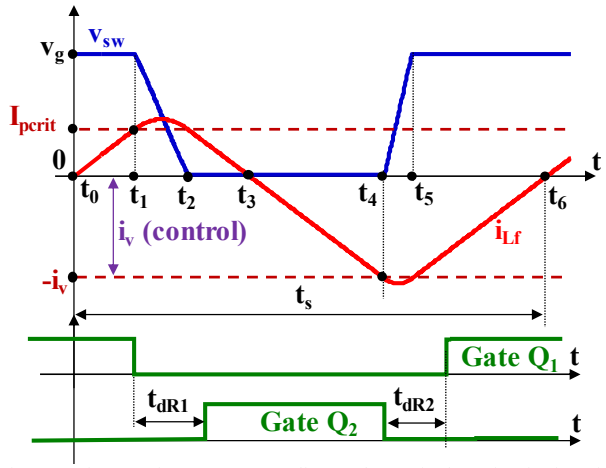

Fig. 7. Main waveforms corresponding to the equivalent circuit given in Fig. 2 working in sink mode.

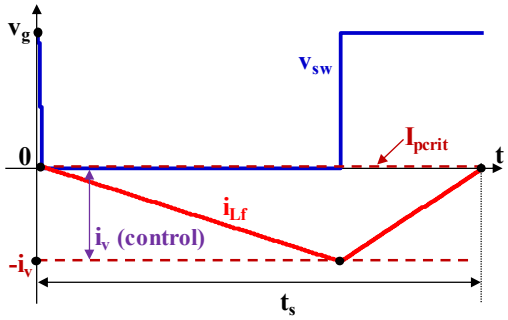

Fig. 8. Main operating waveforms at heavy load in sink mode.

$$G_{gvo} = {L_f}^2 \frac{F_0}{V_g}\left[1 + \frac{{V_o}^2}{{Z_c}^2 {I_v} I_{pcrit}}\right], \tag{115}$$

$$G_{giv} = {L_f}^2 \frac{F_0 V_o}{V_g(I_v - I_{pcrit})}\left[1 + \frac{(V_g - V_o)V_o(2I_v - I_{pcrit})}{{Z_c}^2 {I_v}^2 I_{pcrit}}\right], \tag{116}$$

$$F_0 = -\frac{1}{2{T_s}^2} \cdot \frac{(I_v + I_{pcrit})^2 (I_v - I_{pcrit}) {V_g}^2}{(V_g - V_o)^2 {V_o}^2}. \tag{117}$$

The heavy load simplification is feasible in this case as well. Equations (100), (101), (103), (104), (106) remain invariable in this case, but (99), (102), (105) and (107) become:

$$T_s = \frac{L_f I_v V_g}{(V_g - V_o)V_o}, \tag{118}$$

$$G_{iiv\_hl} = \lim_{\lambda \to 0} G_{iiv} = -\frac{1}{2}, \tag{119}$$

$$G_{gip\_hl} = \lim_{\lambda \to 0} G_{gip} = -\frac{1}{2}\left(\frac{V_o}{V_g}\right), \tag{120}$$

$$I_o = -\frac{I_v}{2}. \tag{121}$$

It is important to note that $i_v > i_{pcrit}$ (and, therefore, $I_v > I_{pcrit}$) in sink mode, making F_0 become negative. This means all the G parameters also reverse their sign with respect to the source mode operation. This is directly appreciated in the case of (119) and (120) and can be easily deduced in the other cases because I_o and R_o become negative.

From these parameters, the following useful transfer functions, that can be directly obtained:

$$\left.\frac{\hat{v}_o}{\hat{v}_g}\right]_{\substack{\hat{\imath}_v=0 \\ \hat{\imath}_{sink}=0 \\ \hat{\imath}_{source}=0}} = \frac{G_{ivg} R_{eq}}{1 + R_{eq} C_f s}, \tag{122}$$

$$\left.\frac{\hat{v}_o}{\hat{\imath}_v}\right]_{\substack{\hat{v}_g=0 \\ \hat{\imath}_{sink}=0 \\ \hat{\imath}_{source}=0}} = \frac{G_{iiv} R_{eq}}{1 + R_{eq} C_f s}, \tag{123}$$

$$\left.\frac{\hat{v}_o}{\hat{\imath}_{source}}\right]_{\substack{\hat{\imath}_v=0 \\ \hat{v}_g=0 \\ \hat{\imath}_{sink}=0}} = \frac{R_{eq}}{1 + R_{eq} C_f s}, \tag{123}$$

Finally, the study carried out for the buck convert can be easily extended to the boost converter, also working in source and sink modes. To do this, the position of the voltage source and of the parallel connection of output capacitor and the load must be interchanged in Fig. 4. Therefore, current i_g will be now the current injected into the parallel connection of the output capacitor and the load. According to the direction selected for currents i_{Lf}, i_o and i_g in Fig. 2, these quantities become negative in source mode and positive in sink mode for the boost converter. As a consequence, control variable i_v will be used in source mode, whereas i_p will be the control variable in sink mode. The values of G parameters will be the ones corresponding to the control variable used: equations (111) – (117) in source mode and equations (92) – (98) in sink mode. Dynamic resistor r_1, instead of r_2, must be used now in (108) to calculate the equivalent resistance R_{eq}, which is of primary concerns to compute the converter transfer functions. Heavy load simplifications are also possible in this case.

V. Experimental Results

The small signal model is validated by testing a buck and a boost converter. Their main specifications are summarized in Table I and a picture of one of them is depicted in Fig. 9. The controller stage has been implemented following [8]. The control to output voltage transfer function has been measured with a frequency response analyzer, model FRA6340 from Venable.

Table I. Components and main specifications for buck and boost prototypes.

Parameter	Buck prototype	Boost prototype
V_{in} [V]	48	24
V_o [V]	24	48
P [W]	±80	±100
Inductance [µH]	69.6, RM8, N97, EPCOS. Litz wire 0.3mm. 97 turns	33, SER2918H-333KL. Coilcraft
Output capacitance [µF]	445	450
Transistors	TPH7R006PL, Toshiba 60V, 60A, 8.9mΩ	
Switch driver	ISL6700, Intersil	
Current sensor	CQ-3200. Hall-effect. AKM Semiconductors	

As a couple of examples, Fig. 10 and Fig. 11 show two Bode plots corresponding to operate in source mode. The first one

corresponds to the buck converter prototype operating at medium load (25 W), whereas the second one corresponds to the boost converter prototype at light load (5 W). As these figures show, the measured plots and the predicted ones fit very well. In the case of light load operation (boost converter at 5 W), the most elaborate model fits better with the measured plots than the simpler one. All of these plots have been obtained using a purely resistive load.

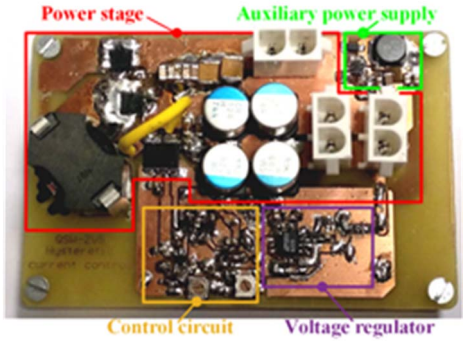

Fig. 9. Picture of the buck converter prototype.

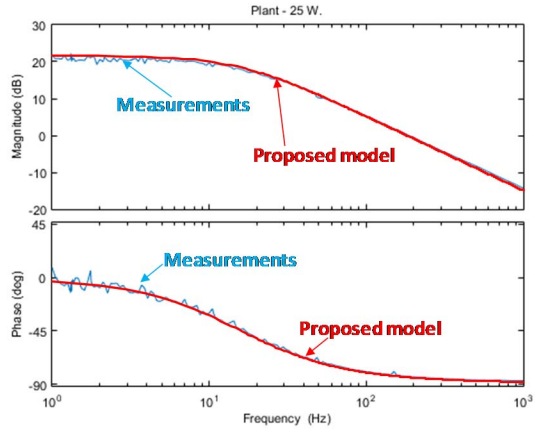

Fig. 10. Bode plots corresponding to the buck converter prototype working in sorce mode at medium load (25 W). The load was resistive.

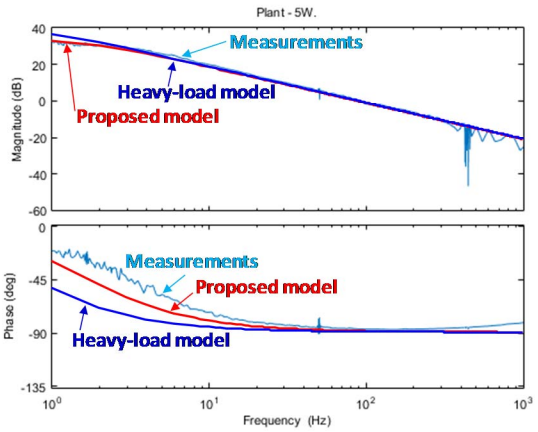

Fig. 11. Bode plots corresponding to the boost converter prototype working in sorce mode at light load (5 W). The load was resistive.

VI. CONCLUSIONS

A couple of small signal models for buck and boost converters operating in Triangular Current Mode (TCM) and controlled with a variable-width Hysteretic Current Mode Control (HCMC) have been proposed in this paper. The first model takes into account the resonant intervals that occur at the end of the transistors conduction periods. As the switching frequency of these converters is low at heavy load, the duration of these intervals is negligible in this condition and a much simpler model can be used at heavy load (and even at medium load). Just on the other hand, the switching frequency is much higher when the converters are operating at light load. Due to this, the first model must be used in this condition. Both models correspond to simple first order systems, which is a consequence of using a control system that resets the inductor current to a specific value each switching cycle.

The most elaborate model (the first one) is based on assuming constant inductor current during the resonant intervals. In this model, the duration of the resonant intervals correspond to the actual time that the transistors output capacitances take to interchange their electric charge. It should be noted that this electric charge only depends on the voltage variation across these capacitances (which is the input voltage in the case of the buck converter and the output voltage in the case of the boost converter) and on the transistors output capacitances. The value of this electric charge is directly provided in many transistor data sheets.

REFERENCES

[1] V. Vorperian, “Quasi-square-wave converters: topologies and analysis,” *IEEE Transactions on Power Electronics*, vol. 3, no. 2, Apr. 1988, pp. 183–191.

[2] C. Marxgut, J. Biela, and J. W. Kolar, “Interleaved triangular current mode (TCM) resonant transition, single phase PFC rectifier with high efficiency and high power density,” in *Proc. Int. Power Electronics Conf. - ECCE ASIA -*, Jun. 2010, pp. 1725–1732.

[3] D. Maksimovic, “Design of the zero-voltage-switching quasi-square-wave resonant switch,” in *Proc. 24th Annual IEEE Power Electronics Specialists Conf. PESC '93 Record*, Jun. 1993, pp. 323–329.

[4] B. Ray and A. Romney-Diaz, “Constant frequency resonant topologies for bidirectional DC/DC power conversion,” in *Proc. 24th Annual IEEE Power Electronics Specialists Conf. PESC '93 Record*, Jun. 1993, pp. 1031–1037.

[5] R. Kollman, J. Betten, and B. S. Lee, “Power supply solution for DDR bus termination,” Analog Applications, 2001.

[6] M. Orabi, A. Ghahary and A. Lotfi, "Operating Limitation of Buck Power Supplies Feeding DDR Memories -Source-Sink-Mode," *2007 IEEE Power Electronics Specialists Conference*, Orlando, FL, 2007, pp. 363-369.

[7] M. Rodriguez, G. Stahl, L. Corradini, and D. Maksimovic, “Smart DC power management system based on software-configurable power modules,” *IEEE Transactions on Power Electronics*, vol. 28, no. 4, Apr. 2013, pp. 1571–1586.

[8] A. Vazquez, K. Martin, M. Arias and J. Sebastian, "A very simple analog control for QSW-ZVS source/sink dc-dc converters with seamless mode transition," *2019 IEEE Applied Power Electronics Conference and Exposition (APEC)*, Anaheim, CA, USA, 2019, pp. 220-226.

[9] P.R.K. Chetty, "CIECA: Application to Current Programmed Switching Dc-Dc Converters". *IEEE Transactions on Aerospace and Electronic Systems,* vol. AES-18, no. 5, September 1982, pp. 538-544.